Sensors and Materials, Vol. 34, No. 10 (2022) 3781–3796
MYU Tokyo

S & M 3076

Analysis of Deep Drawing Process for Micro Square Holes on Copper Sheets

Tsung-Chia Chen,[1] Ching-Min Hsu,[1] Cheng-Chi Wang,[2*] and Tsui-Er Lee[3]

[1]Department of Mechanical Engineering, National Chin-Yi University of Technology,
No. 57, Sec. 2, Zhongshan Rd., Taiping Dist., Taichung 411030, Taiwan
[2]Graduate Institute of Precision Manufacturing, National Chin-Yi University of Technology,
No. 57, Sec. 2, Zhongshan Rd., Taiping Dist., Taichung 411030, Taiwan
[3]Office of Physical Education, Asia University,
No. 500, Lioufeng Rd., Wufeng, Taichung 41354, Taiwan

(Received May 26, 2022; accepted September 27, 2022)

Keywords: micro deep drawing, springback, copper, material deformation history

For the design and fabrication of dies by the deep drawing process, the problems of springback after load removal and the formation of cracks must be considered. In this study, a deep drawing process for micro square holes on copper sheets was analyzed on the basis of an updated Lagrangian formulation and 3D finite element analysis. Sheet behavior was simulated using a micro-elastoplastic material model, the performance of which was compared with that of models involving conventional materials. Subsequently, Dynaform software was used for simulation analysis to obtain the material deformation history as well as determine the thickness change distribution and the maximum stress and strain of a copper sheet. It was found that the punch fillet radius and forming ratio affect the relationship between the punch load and the punch stroke, the distributions of stress and strain, and the maximum flange height. Finally, simulation results were compared with experimental results to confirm the accuracy of the 3D finite element analysis of the elastoplastic deformation. The results show the effect of the punch fillet radius for copper sheets on the drawing process: when the punch fillet radius is small, the punch load increases and decreases more rapidly. The maximum stress and strain decrease as the punch fillet radius increases. These findings serve as a valuable reference for design and processing by micro deep drawing.

1. Introduction

Deep drawing is a special process in sheet metal forming that is capable of forming many metallic parts and structures, and it has a wide range of applications in the packaging, automotive, and aerospace industries. During the forming process, insufficient formability or improper parameter setting may generate defects, such as fractures and excessive local thinning or wrinkling, which may reduce the precision of the workpiece. Life and yield must be

*Corresponding author: e-mail: wccpipn@gmail.com
https://doi.org/10.18494/SAM4082

ISSN 0914-4935
https://myukk.org/

compensated for in the mold design stage. The miniaturization of the sheet is affected by the scale effect; thus, the parameters that must be controlled differ from those in general forming, such as the surface roughness of the element, the friction during the forming process, the plastic flow stress of the material, and springback. Therefore, the accurate prediction and control of the parameters in the micro-forming process are essential.[1–3]

Sheet metal forming is currently divided into four basic models,[4] namely, stretching, drawing, stretch-flanging, and bending. A sheet metal is subjected to different forces for different forming models, and various formability tests are utilized to evaluate the formability of sheet metal in an actual stamping. In the forming process, fracture, local overthinning, or wrinkling could occur in a sheet metal because of poor formability or inappropriately set processing parameters, which is an issue that has been explored by researchers and experts. Square hole-flanging is a type of sheet metal stretching,[5] and the products can be applied to the components of automobiles, the inner plates of airplanes, pipe connections, and general household appliances. In general sheet metal forming, the processing parameters are acquired by trial and error or on the basis of experiences in general die factories, meaning that it has not been possible to control the data for use in process design. When the square hole-flanging can be pre-simulated to optimize the processing parameters, thus replacing trial and error in general die factories, the labor, time, and cost of correcting errors can be reduced.

Worswick and Finn[6] simulated the forming of round, square, and Z hole flanges using the explicit dynamic finite element method. They combined the forming limit diagram with the von Mises, Hill, and Barlat yield criteria to discuss the forming limit of sheet metal. Huang and Chien[7] analyzed the forming limit of a cylindrical punch radius in hole-flanging by numerical analysis; the effect of the punch contour radius on the forming limit was negligible, but the effect on the punch load was large. Leu *et al.*[8] compared the maximal punch load in hole-flanging for various geometric punch shapes (cone, hemisphere, and cylinder) while changing some of the processing parameters in a numerical simulation. The experimental results showed that the greatest punch load in forming was for the cylindrical punch, although the cone punch exhibited a smaller strain hardening index, larger friction coefficient, larger forming load, larger punch angle, and larger forming load.

In 2022, Kabakçı and Demirel[9] experimentally investigated the mechanical formability of Al6061-T6 sheet material using a pre-bulging process. They applied an innovative die entrance design to conventional deep drawing dies and analyzed the formability of the Al6061-T6 material, as well as the effects of the innovative design on the energy consumption and thickness distribution. Chen *et al.*[10] presented a procedure to establish and validate numerical process models through an investigation of the deep drawing of AA1100-O blanks using a 3D servo press. They studied the robustness of deep-drawing simulation models to different process variations and performed experiments on a 3D servo press equipped with a spring-loaded blank holder. From the experiments, they obtained the force–displacement characteristic of the punch, as well as local features, flange draw-in, and wall thinning.

In this study, we analyzed the deep drawing process of micro square holes on copper sheets by simulations and experiments. We investigated the deformation behavior of a flange with a micro square hole in stretch-forming using the finite element analysis software Dynaform to

simulate the stretch-forming process. The experiments were performed to confirm and analyze the results, specifically to determine whether Dynaform can be accurately applied to stretch-forming, to promote its use in relevant factory procedures, and to provide stretch-forming parameters.

2. Principle and Theory Analysis

We make several basic assumptions for the copper sheet subjected to elastoplastic deformation considered in the present study.

- The material is homogeneous and planar anisotropic.
- The material satisfies Hooke's law in the elasticity area.
- Dies are regarded as rigid bodies.
- The effects of temperature and residual stress are not considered in the material forming.

We use the updated Lagrangian formulation (ULF) under finite deformation for various metal forming processes. The Jaumann differential of the Cauchy stress is used for the stress rate of the constitutive equation; therefore, the updating virtual work equation can be obtained as follows:[11]

$$\int_{V^E}\left(\sigma_d - 2\sigma_d\dot{\varepsilon}_c\right)\delta\dot{\varepsilon}_c dV_d + \int_{V^E}\sigma_d V_{GM}\delta V_{GM} dV = \int_{S_f}\dot{F}\delta v ds_d \,. \tag{1}$$

Here, σ_d is the Jaumann differential of Cauchy stress, $\dot{\varepsilon}_c$ is the Cauchy strain rate tensor, V_{GM} is the velocity gradient matrix, v is the velocity, ds_d is the differential surface area after deformation, $\dot{F}$ is the rate of change in force, and dV_d is the differential volume after deformation.

Because the thickness of the sheet is less than 1.0 mm, the size effect should be considered. Thus, a new material model must be established for the micro-forming process, and the traditional Swift material model is applied to modify the stress–strain relationship as follows:[12]

$$\sigma_m\left(t,\overline{\varepsilon}\right) = a\varphi e^{bt}\left(\varepsilon_0 + \overline{\varepsilon_p}\right)^{n\left(ce^{dt}-1\right)}, \tag{2}$$

where a, b, c, and d are correction values and t is the sheet thickness.

We substitute the values for a, b, c, and d obtained from the research of Liu[13] in Eq. (2) to give

$$\sigma_m\left(t,\overline{\varepsilon}\right) = 0.73667\varphi e^{0.3152t}\left(\varepsilon_0 + \overline{\varepsilon_p}\right)^{n\left(1.0106e^{-0.01029t}-1\right)}. \tag{3}$$

The modified material model in Eq. (3) is used in finite element analysis in this study, and experiments are then implemented to verify the validity of the model Eq. (3).

3. Numerical Simulations and Experiments

The shell elements of the four nodes of a quadrangle are applied to deduce the stiffness matrix. These elements are processed with a CAD package, and mash segmentation is performed on the established blank shape for the numerical analysis in the elastoplastic 3D finite element program. The simulation results are output to the CAD package for analysis, and the output results are displayed as a deformation diagram and a stress–strain distribution. The coefficient of friction, sheet thickness, and punch fillet radius are changed as parameters to determine the relationship between the punch load and the punch stroke, the distributions of the maximal stress and maximal strain, and the thickness distribution.

3.1 Numerical simulation

The numerical simulation process is as follows:

1. Draw and confirm the 3D models of the dies and sheet.
2. Mesh the 3D model and perform preprocessing using Dynaform.
3. Set the process parameters of the dies and the sheet data files using Dynaform and conduct numerical analysis with the LS-DYNA program.
4. Complete the postprocess calculations and output the results.
5. Compare the data obtained from the numerical analysis and experiment.

The friction coefficient μ of 0.1 set in the simulation was close to the actual friction value obtained.[14,15] The simulation results for punch load, punch stroke, stress, and strain were output to Dynaform for postprocessing and subsequent analysis. During the postprocessing, we examined the deformation history diagram and the stress and strain distribution diagrams for different punch strokes in each stage. These data can serve as a reference for mold design and drawing procedures to determine the probability of cracks or wrinkles and reduce the high financial and time costs associated with the conventional trial-and-error method.

3.2 Experiments

Figure 1 presents the stretch module of a flange with a micro square hole and a copper sheet. The relevant parameters of the experiments are shown in Table 1.[16,17] The mechanical properties and material parameters of copper are shown in Table 2.[16,18]

3.2.1 Experimental setup

Figure 2(a) shows the die components, where the punch has a hierarchical design to enhance its rigidity. Tool steel (SKD11) is utilized for the die to improve its rigidity and wear resistance. Figure 2(b) displays copper sheets before micro hole flange drawing. Since the initial thickness of each test copper sheet is low, the thickness after the deep drawing experiment is measured using a laser displacement sensor (Keyence LC-2430).

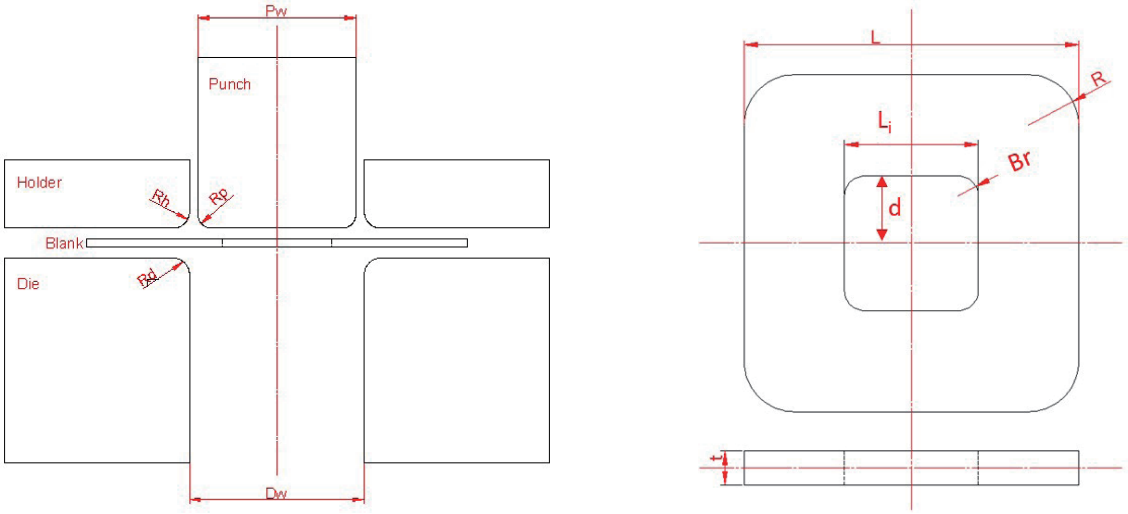

(a) (b)

Fig. 1. (Color online) Parameters and specifications of (a) stretch module of flange with micro square hole and (b) copper sheet.[16,17]

Table 1
Relevant parameters (unit: mm).

	Model 1	Model 2	Model 3		Model 1	Model 2	Model 3
P_W	10.00	5.00	2.50	L_i	20	10	5
D_W	10.44	5.22	2.61	R	9	4.5	2.25
R_p	1.00	0.50	0.25	Br	5	2.5	1.5
R_d	1.20	0.60	0.30	t	1.6	0.8	0.4
L	20	10	5				

Table 2
Mechanical properties and material parameters of copper.

Material	E (GPa)	v	σ_y (MPa)	K (MPa)	n	ε_0
Model 1	26400	0.3	887	1161	0.82	0.41
Model 2	19700	0.3	586	989	0.71	0.48
Model 3	25000	0.3	225	565	0.21	0.01

E: Young's modulus; v: Poisson's ratio; σ_y: yielding stress.

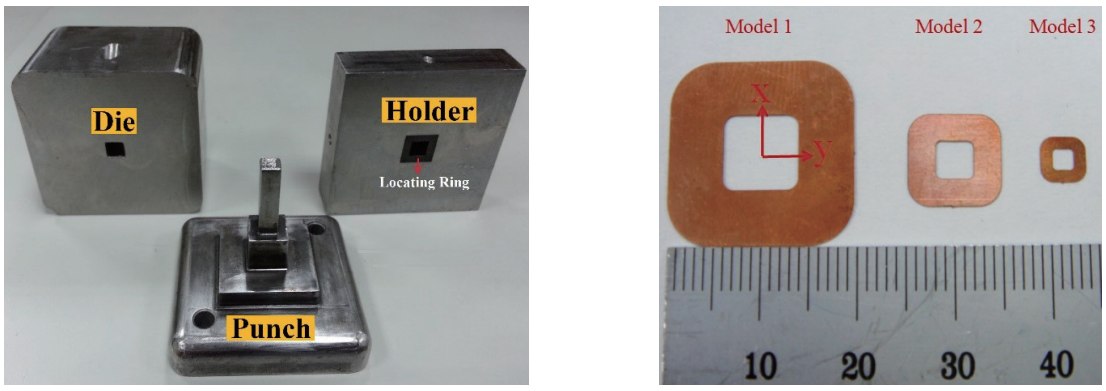

(a) (b)

Fig. 2. (Color online) (a) Key components of mold and (b) C1100 copper applied in experiment before drawing.[16,17]

4. Results and Discussion

4.1 Effect of punch fillet radius

The punch fillet radius is changed to analyze the process, and the copper sheet is regarded as an isotropic material. The situation after the last stroke and springback is discussed in this section.

Figure 3 shows the relationship between the punch load and the punch stroke for different punch fillet radius (R_P) values. As shown in the figure, when R_P is small, the punch load

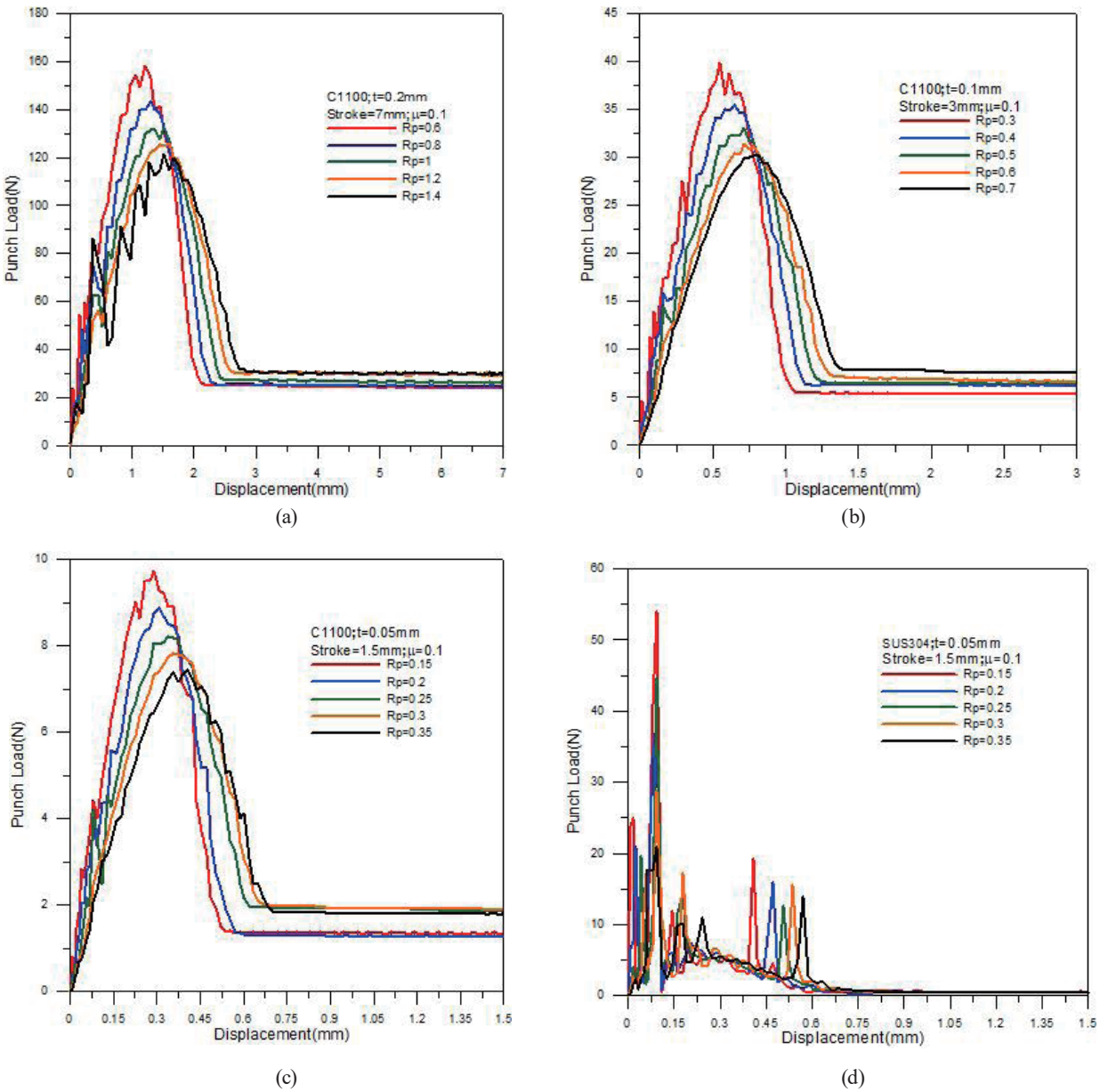

Fig. 3. (Color online) Relationship between punch load and punch stroke for different punch fillet radius values for copper in (a) Model 1, (b) Model 2, and (c) Model 3. (d) Relationship for stainless steel in Model 3.[17,18]

increases and decreases more rapidly. The maximum punch loads required for copper and stainless steel sheets in Model 3 are 9.8 and 54.9 N.[17,18] Accordingly, in Model 3, the punch load required for the stainless steel sheet is 5.6 times that for the copper sheet under the same process parameters as shown in Figs. 3(c) and 3(d).

Figures 4(a)–4(c) show the relationship between R_P and the minimum thickness of the copper sheet. As shown in Fig. 4(d), in Model 3, the copper sheet after the process has a lower minimum thickness than the stainless steel sheet under the same operation parameters.[17,18] The maximum thinning rate is 24.8% for the stainless steel sheet[17,18] and 29.2% for the copper sheet.

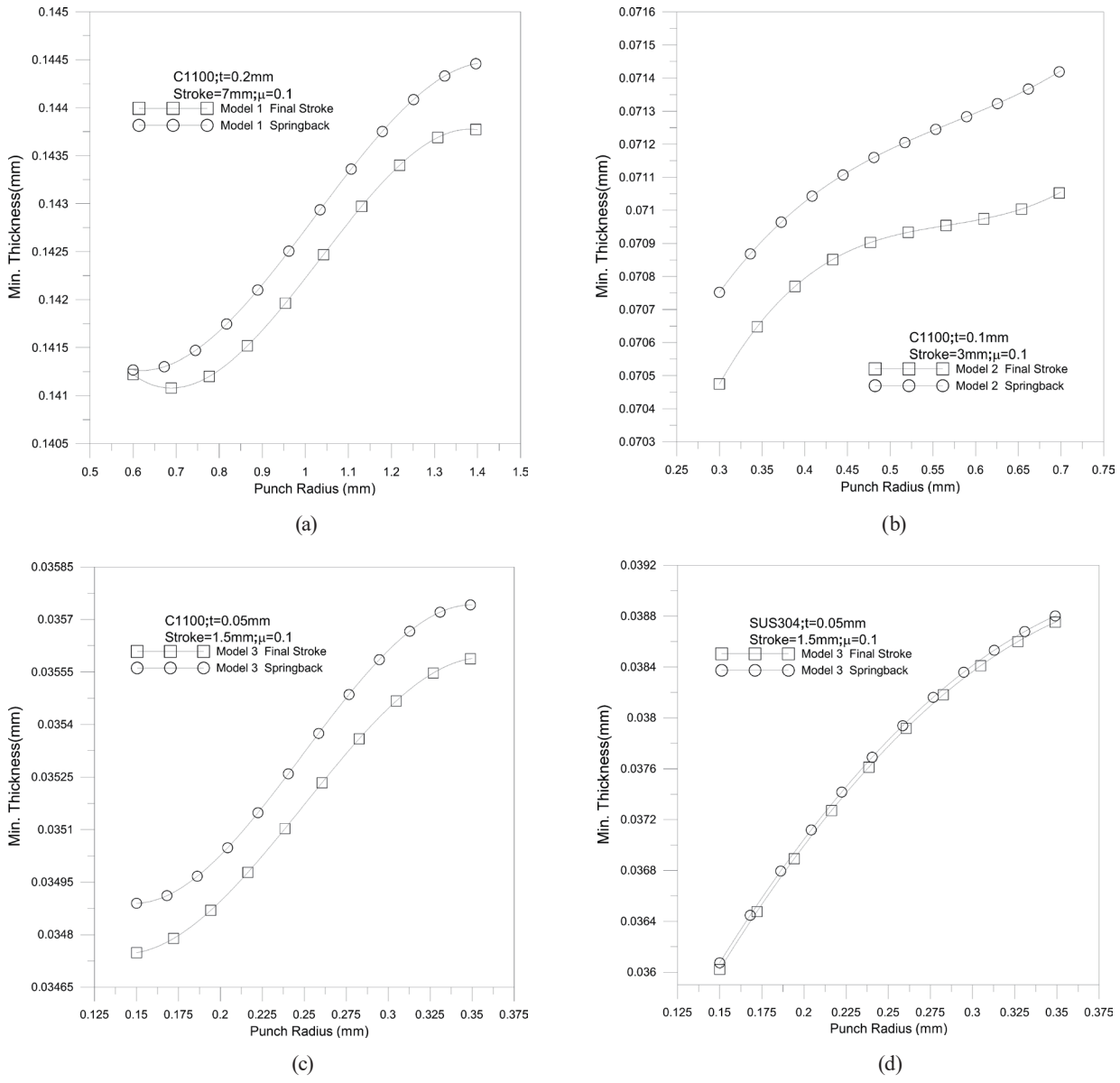

Fig. 4. Relationship between minimum thickness and punch fillet radius for copper in (a) Model 1, (b) Model 2, and (c) Model 3. (d) Relationship for stainless steel in Model 3.[17,18]

Figures 5(a)–5(c) show the relationship between the maximum flange height of the copper sheet and R_P. As shown in Fig. 5(d), for Model 3, the flange height of the copper sheet is slightly larger than that of the stainless steel sheet.[17,18] After unloading and rebounding, the amount of rebound of the copper sheet is slightly smaller than that of the stainless steel sheet.

Figures 6(a)–6(c) show the relationship between the maximum stress and R_P for the copper sheet. As shown in Fig. 6(d), compared with that of the stainless steel sheet in Model 3,[17,18] the

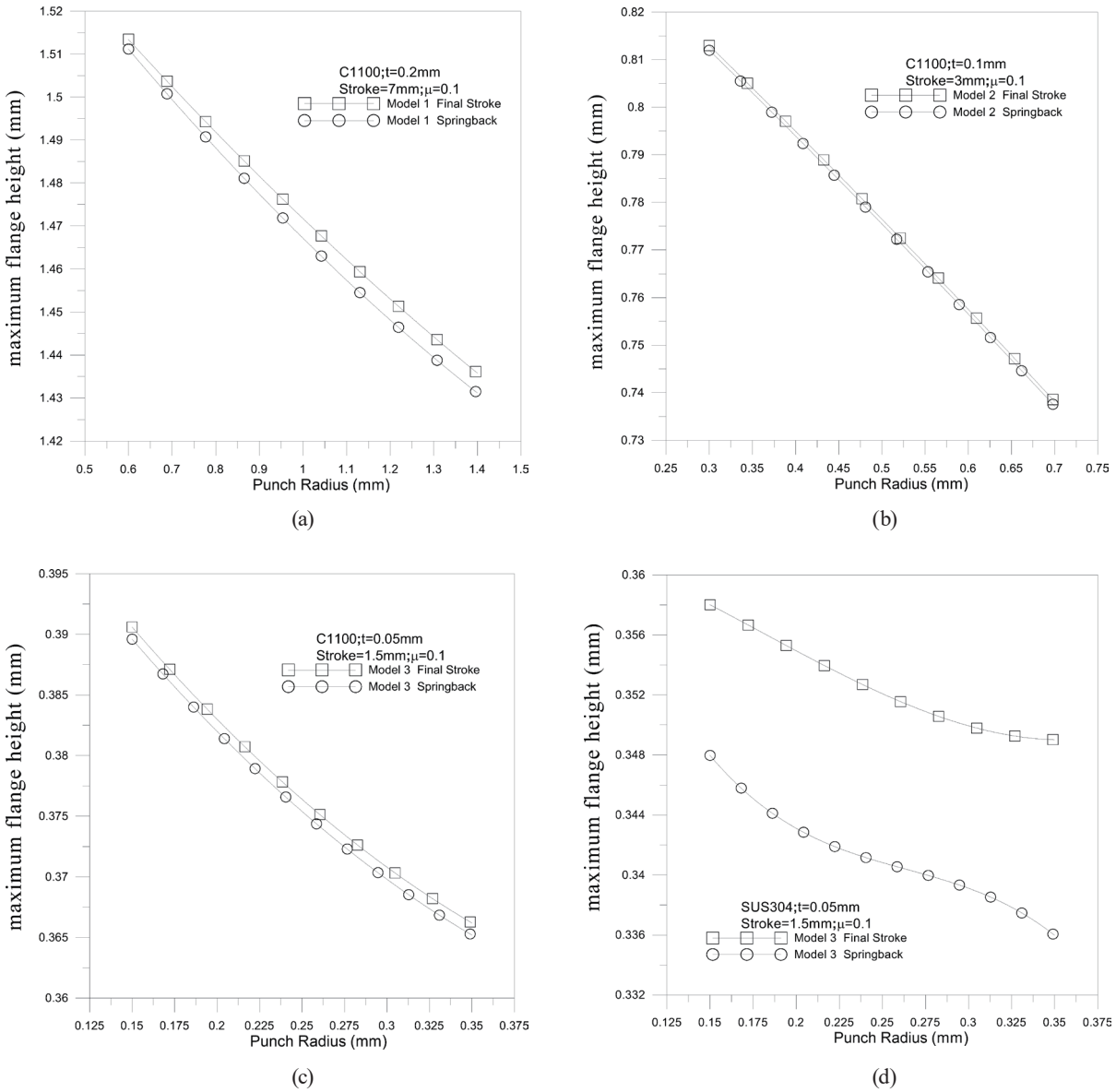

Fig. 5. Relationship between maximum flange height and punch fillet radius for copper in (a) Model 1, (b) Model 2, and (c) Model 3. (d) Relationship for stainless steel in Model 3.[17,18]

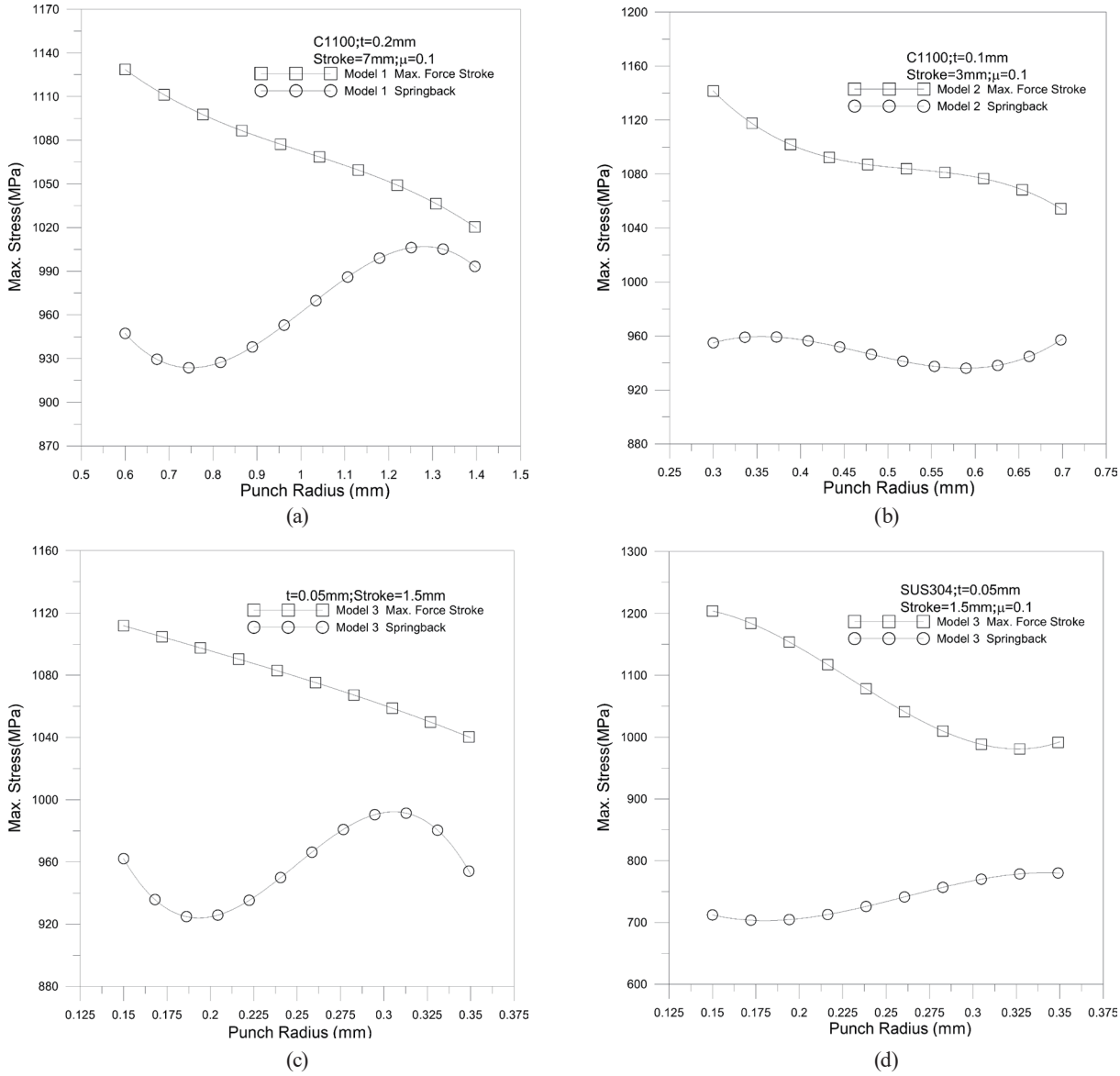

Fig. 6. Relationship between maximum stress and punch fillet radius for copper in (a) Model 1, (b) Model 2, and (c) Model 3. (d) Relationship for stainless steel in Model 3.[17,18]

maximum stress of the copper sheet is small. The stress is then released and reduced after the punch springs back from the flange.

Figures 7(a)–7(c) show the relationship between the maximum strain and R_P for the copper sheet. As shown in Fig. 7(d), compared with the stainless steel sheet in Model 3,[17,18] the copper sheet has a greater amount of strain due to the higher formability of copper and the inherently larger deformation. The strain decreases slightly after unloading and rebounding.

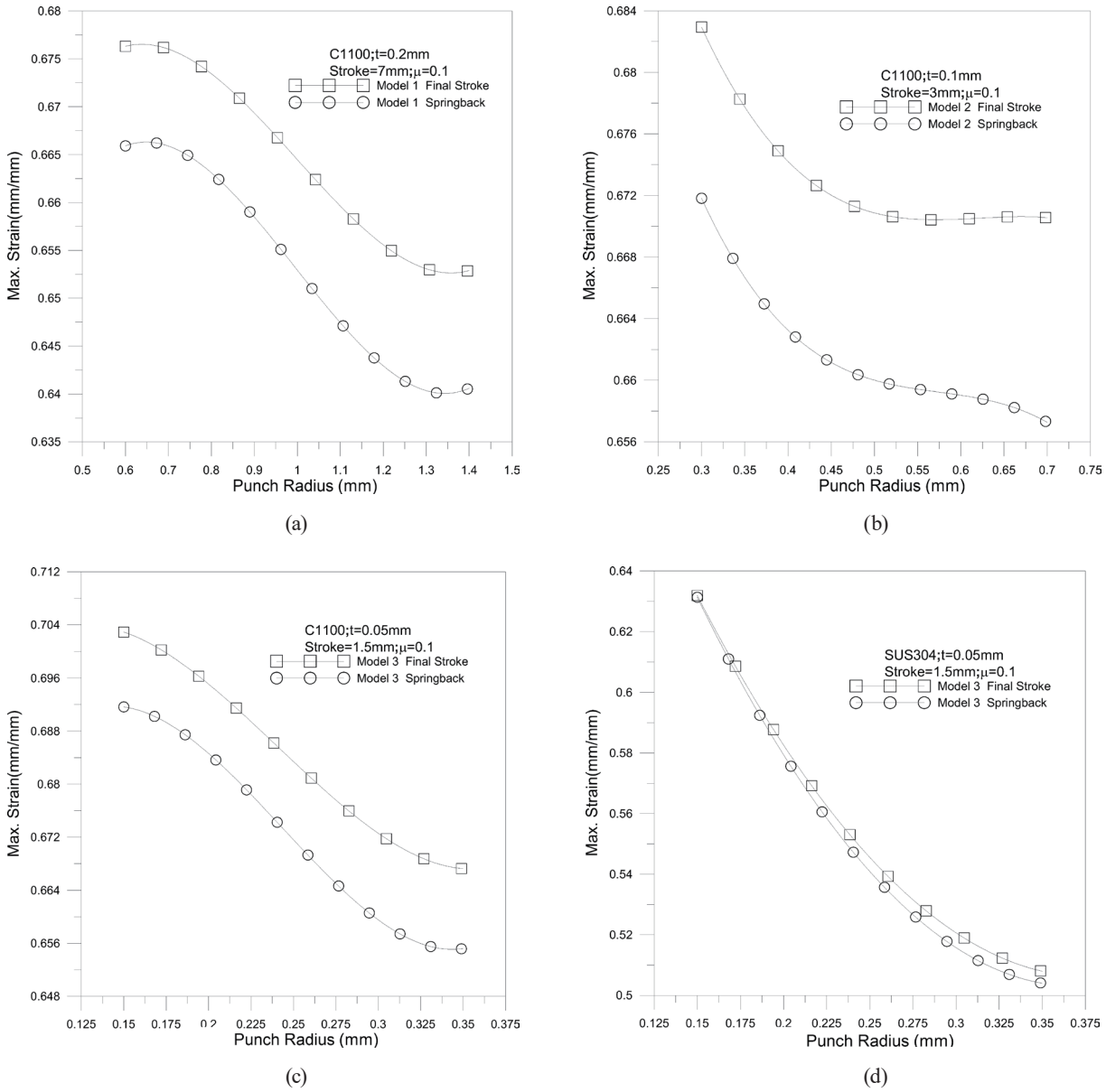

Fig. 7. Relationship between maximum strain and RP for copper sheet in (a) Model 1, (b) Model 2, and (c) Model 3. (d) Relationship for stainless steel in Model 3.[17,18]

4.2 Effect of forming ratio for copper sheets on drawing process

The forming ratio (*FR*) was changed to simulate the external effect on the forming process. *FR* is defined as

$$FR = Ah/Ap, \tag{4}$$

where *Ap* and *Ah* are the sectional areas of the square punch and square hole before processing, respectively.

The material parameters are shown in Table 1, where the materials are regarded as isotropic during analysis. Copper sheets of different thickness are processed, and it is found that a crack occurs at the edge of the flange when *FR* decreases to 0.81 as shown in Fig. 8.

In the following section, *FR* of the copper sheet is set to 0.82, 0.84, 0.86, 0.88, and 0.9 to analyze its effect on the drawing process. The last stroke for deep drawing and the springback are discussed as follows.

Figures 9(a)–9(c) show the relationship between the load and stroke of the punch with different *FR* values for the copper sheet. Through the analysis, it is found that the forming limit decreases at *FR* = 0.82. For a smaller *FR*, a longer stroke is required to pass through the sheet.

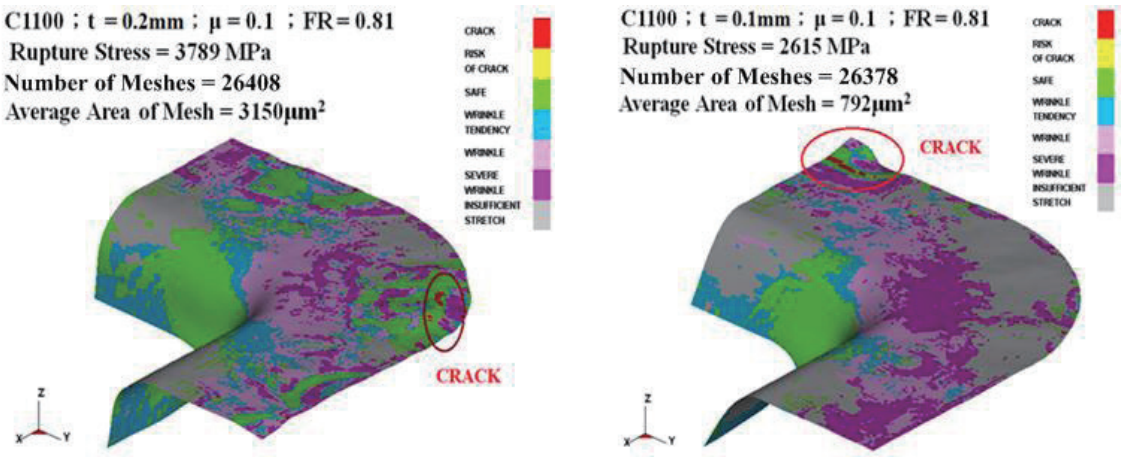

(a)

(b)

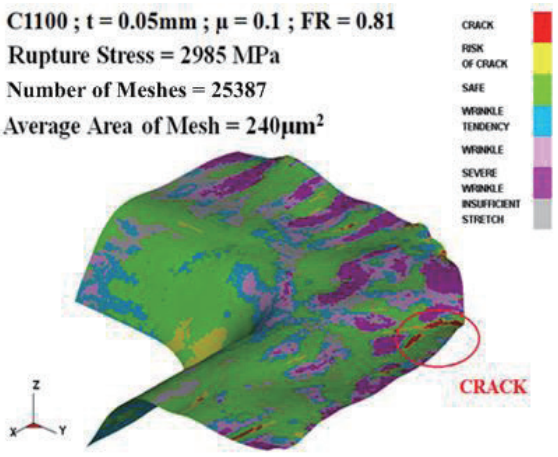

(c)

Fig. 8. (Color online) Forming limit of sheet material: (a) Model 1, (b) Model 2, and (c) Model 3.

The process for the copper sheet in Model 3 has a lower punch load than that for the stainless steel sheet,[17,18] as shown in Fig. 9(d).

For Model 3 with the same parameters of the copper and stainless steel sheets, the maximum punch load of the copper sheet is 14.1 N, compared with 80 N for the stainless steel sheet, as shown in Figs. 9(c) and 9(d).

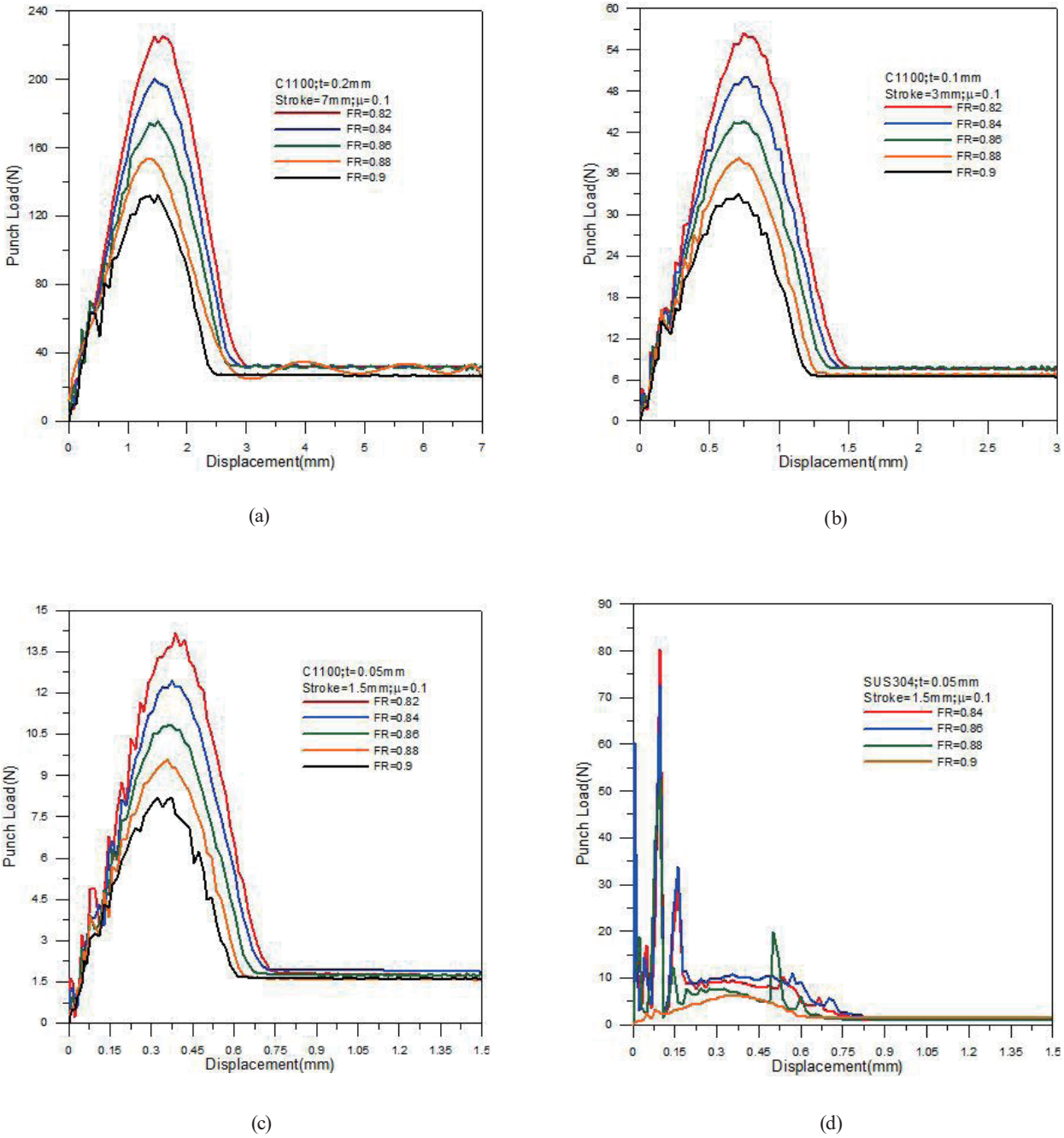

Fig. 9. (Color online) Relationship between load and stroke of punch with different *FR* values for copper in (a) Model 1, (b) Model 2, and (c) Model 3. (d) Relationship for stainless steel in Model 3.[17,18]

The relationship between the maximum stress in the flange of the copper sheet and *FR* is shown in Figs. 10(a)–10(c). The copper sheet has a smaller maximum stress than the stainless steel sheet,[17,18] as shown in Fig. 10(d). The stress is then released and reduced after the punch springs back from the flange.

Figures 11(a)–11(c) reveal the relationship between *FR* and the maximum strain in the flange of the copper sheet. The copper sheet has a larger maximum strain than the stainless steel

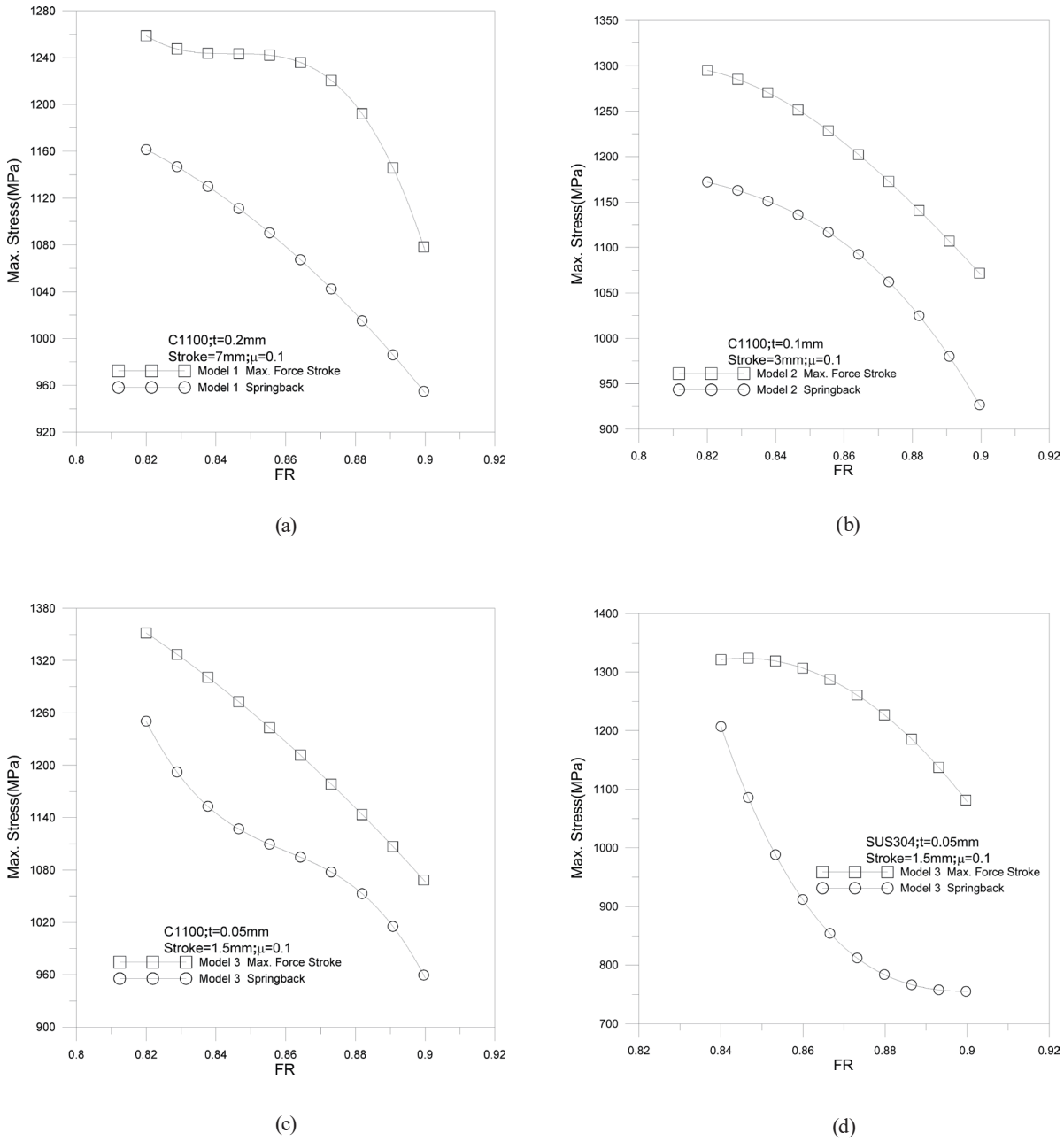

Fig. 10. Relationship between maximum stress in flange and *FR* in (a) Model 1, (b) Model 2, and (c) Model 3. (d) Relationship for stainless steel in Model 3.[17,18]

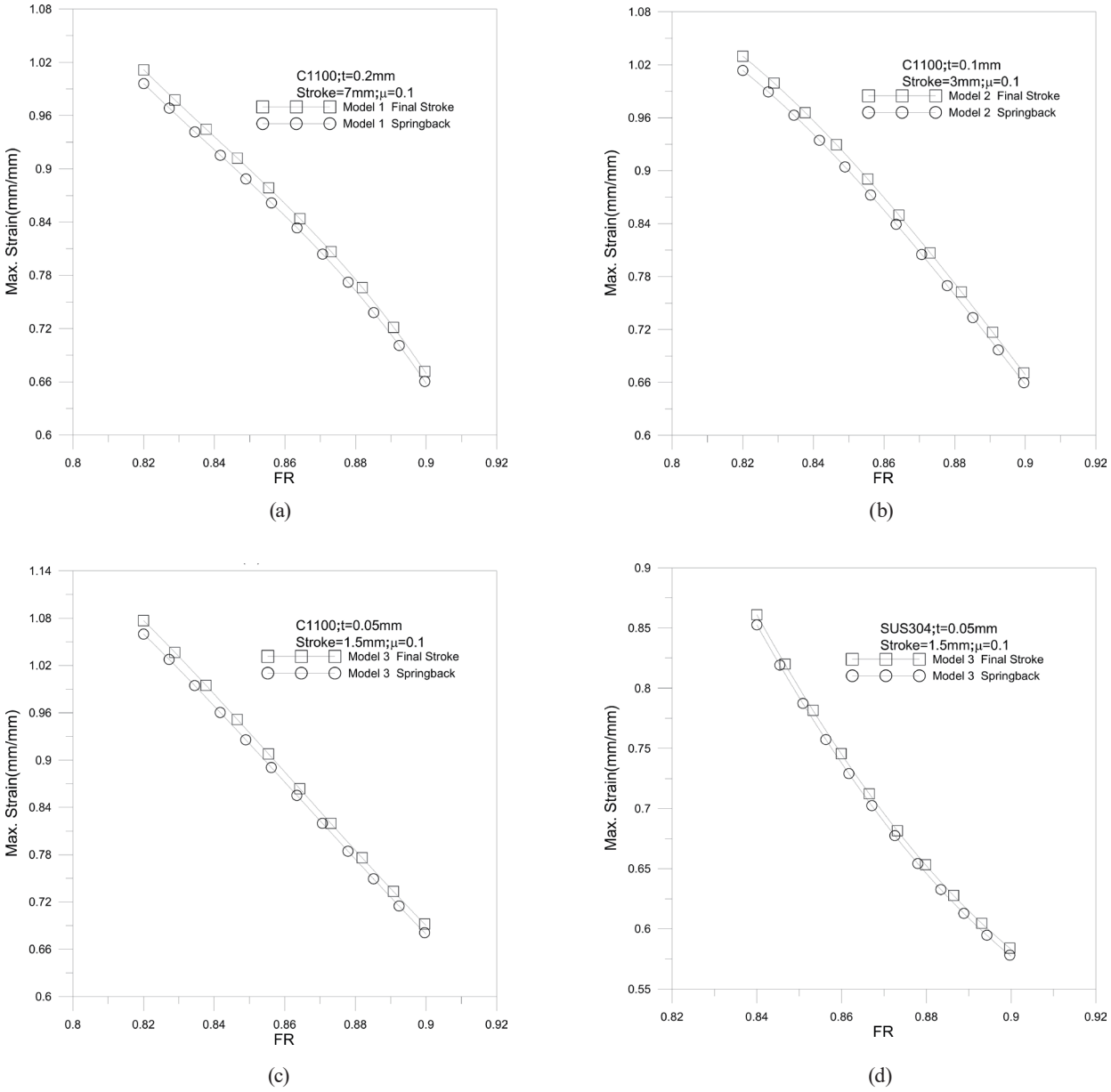

Fig. 11. Relationship between *FR* and maximum strain in flange for copper in (a) Model 1, (b) Model 2, and (c) Model 3. (d) Relationship for stainless steel in Model 3.[17,18]

sheet,[17,18] as shown in Fig. 11(d). There is a slight decrease in strain after the punch is retracted and rebounds.

Figures 12(a)–12(c) show the relationship between the maximum height of the flange and *FR*. The flange height for the copper sheet is slightly larger than that for the stainless steel sheet,[17,18] as shown in Fig. 12(d). After unloading and rebounding, the amount of rebound for the copper sheet is slightly smaller than that for the stainless steel sheet.

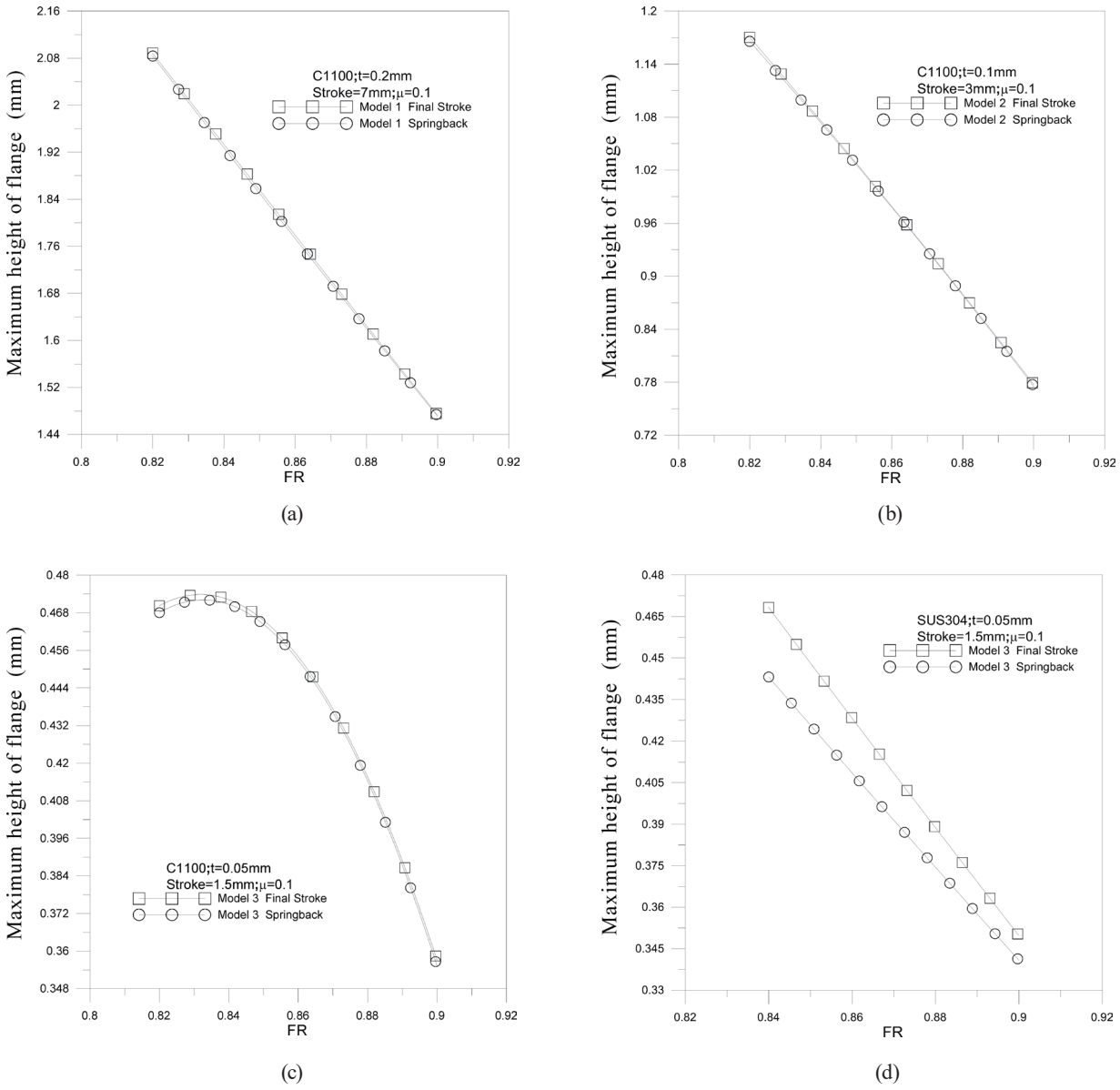

Fig. 12. Relationship between maximum height of flange and *FR* for copper in (a) Model 1, (b) Model 2, and (c) Model 3. (d) Relationship for stainless steel in Model 3.[17,18]

5. Conclusions

The theory of incremental elastoplastic deformation 3D finite element analysis used in this study adopts finite deformation theory and ULF. Dynaform composed of the LS-DYNA solver is employed, and the scale factor is used to establish a new microscopic elastoplastic material model and correct the effect of the scale effect on thin sheets. This elastoplastic deformation finite element analysis method has been verified by experimental comparison and demonstrated to effectively simulate and analyze the complete process of square hole flange stretch-forming.

The following conclusions are obtained by combining the results and discussion of the experimental and simulation analyses.

1. Using this finite element analysis method, the complete deformation process of square hole flange drawing can be accurately analyzed, the deformation history can be fully successfully depicted, and the forming problems in the actual drawing process can be predicted.
2. Using the finite element simulation program, the maximum stress and minimum thickness are predicted to decrease in the area where the blank and the punch corner come into contact. Because this area of the material sheet is subjected to the greatest tensile stress, the thickness of the peripheral edge of the reaming hole is significantly lower, making this area prone to rupture.
3. Using the finite element simulation program, it is predicted that the flange height increases with the fillet radius of the inner hole in a copper sheet. Moreover, by comparing the minimum thickness values, it is found that the forming limit increases with the inner hole fillet radius.
4. From the results of the finite element simulation, it is predicted that the punch load decreases with increasing punch fillet radius when copper sheets are used.
5. From the results of the finite element simulation, it is also predicted that the forming limit of copper is 0.82 when the thickness of the sheet is 1% of the length of the square outside the sheet.
6. The copper sheet has a smaller maximum stress than the stainless steel sheet. The stress is released and reduced after the punch springs back from the flange. In addition, the copper sheet has a larger maximum strain than the stainless steel sheet.

Acknowledgments

This research was funded by the Ministry of Science and Technology of Taiwan (grant number MOST 110–2221-E-167–021).

References

1 I. Aminzahed, M. M. Mashhadi, and M. R. V. Sereshk: Mater. Sci. Eng. C. **71** (2017) 685.
2 W. Phanitwong and S. Thipprakmas: Metals **10** (2020) 870.
3 K. Bouchaâla, M. F. Ghanameh, M. Faqir, M. Mada, and E. H. Essadiqi: Heliyon **7** (2021) e06662.
4 S. Thiruvarudchelvan: J. Mater. Process. Technol. **54** (1995) 355.
5 H, Naceur, Y. Q. Guo, J. L. Batoz, and L. C. Knopf: Int. J. Mech. Sci. **43** (2001) 2407.
6 M. J. Worswick and M. J. Finn: Int. J. Plast. **16** (2000) 701.
7 Y. M. Huang and K. H. Chien: J. Mater. Process. Technol. **113** (2001) 720.
8 D. K. Leu, T. C. Chen, and Y. M. Huang: J. Mater. Process. Technol. **88** (1999) 134.
9 M. O. Kabakçı and M. Y. Demirel: Proc. Inst. Mech. Eng., Part E: J. Process Mech. Eng. Online first (2022) https://doi.org/10.1177/09544089221103496.
10 K. L. Chen, A. Breunig, J. J. Ha, B. L. Kinsey, P. Groche, and Y. P. Korkolis: Int. J. Mater. Form. **15** (2022) 45.
11 R. M. McMeeking and J. R. Rice: J. Solids Struct. **11** (1975) 601.
12 L. Peng, F. Liu, J. Ni, and X. Lai: Mater. Des. **28** (2007) 1731.
13 F. Liu: Postdoctoral Thesis, Shanghai Jiao Tong University, Shanghai, China (2006).
14 J. T. Oden and E. B. Pries: ASME J. Appl. Mech. **50** (1983) 67.
15 M. J. Saran and R. H. Wagoner: ASME J. Appl. Mech. **58** (1991) 499.
16 T. C. Chen, C. M. Hsu, and C. C. Wang: Sens. Mater. **33** (2021) 3563.
17 C. M. Hsu: Master Thesis, National Chin-Yi University of Technology, Taichung, Taiwan, 2013.
18 T. C. Chen, C. M. Hsu, and C. C. Wang: Metals **11** (2021) 1436.